Sudden gap closure across the topological phase transition in $Bi_{2-x}In_xSe_3$

Rui Lou,[1] Zhonghao Liu,[2,3] Wencan Jin,[4] Haifeng Wang,[1] Zhiqing Han,[1] Kai Liu,[1] Xueyun Wang,[5,*] Tian Qian,[6] Yevhen Kushnirenko,[2,7] Sang-Wook Cheong,[5] Richard M. Osgood, Jr.,[4,8] Hong Ding,[6,9] and Shancai Wang[1,10,†]

[1]*Department of Physics, Renmin University of China, Beijing 100872, China*

[2]*Institute for Solid State Research, IFW Dresden, Dresden 01171, Germany*

[3]*State Key Laboratory of Functional Materials for Informatic, SIMIT, Chinese Academy of Sciences, Shanghai 200050, China*

[4]*Department of Applied Physics and Applied Mathematics, Columbia University, New York, New York 10027, USA*

[5]*Rutgers Center for Emergent Materials and Department of Physics and Astronomy, Rutgers University, New Brunswick, New Jersey 08854, USA*

[6]*Beijing National Laboratory for Condensed Matter Physics, and Institute of Physics, Chinese Academy of Sciences, Beijing 100190, China*

[7]*Taras Shevchenko National University of Kyiv, Kyiv 01601, Ukraine*

[8]*Department of Electrical Engineering, Columbia University, New York, New York 10027, USA*

[9]*Collaborative Innovation Center of Quantum Matter, Beijing, China*

[10]*Beijing Key Laboratory of Opto-electronic Functional Materials & Micro-nano Devices, Renmin University of China, Beijing, China*

(Received 25 March 2015; published 28 September 2015)

The phase transition from a topological insulator to a trivial band insulator is studied using angle-resolved photoemission spectroscopy on $Bi_{2-x}In_xSe_3$ single crystals. We first report the complete evolution of the bulk band structures throughout the transition. The robust surface state and the bulk-gap size (∼0.50 eV) show no significant change upon doping for $x = 0.05$, 0.10, and 0.175. At $x \geqslant 0.225$, the surface state completely disappears and the bulk-gap size increases, suggesting a sudden gap closure and topological phase transition around $x \sim 0.175$–0.225. We discuss the underlying mechanism of the phase transition, proposing that it is governed by the combined effect of spin-orbit coupling and interactions upon band hybridization. Our study provides a venue to investigate the mechanism of the topological phase transition induced by nonmagnetic impurities.

DOI: 10.1103/PhysRevB.92.115150 PACS number(s): 71.20.−b, 73.20.At, 71.70.Ej, 71.70.Gm

Topological insulators (TIs), principally three-dimensional (3D) topological crystals, have attracted much attention and led to an upsurge in finding new topological phases of matter. Extensive theoretical and experimental work has been carried out on both the robust surface state (SS) and topological properties of the bulk bands. This body of work now allows distinguishing a TI from a "trivial" band insulator [1–16]. Further, the mechanism of the transition between these two classes of insulators, found by substituting nonmagnetic impurities, has been proposed to be a homogeneous 3D topological phase transition (TPT) scenario, i.e., the so-called linear gap-closure scenario, suggesting that the bulk gap is determined by the spin-orbit coupling (SOC) alone and thus would decrease monotonically along with the decreasing SOC strength in the nontrivial phase. This transition happens when the bulk gap closes and an inversion of the bulk conduction band (CB) and valance band (VB) occurs [1,2,17–20].

Practically, the 3D TPT induced by nonmagnetic impurities could only be realized in few real systems, mainly $TlBi(S_{1-x}Se_x)_2$ and $Bi_{2-x}In_xSe_3$. For $TlBi(S_{1-x}Se_x)_2$, the existence of a critical point between the TI $TlBiSe_2$ and the trivial metal $TlBiS_2$ is observed [21–25]. Upon doping, an unexpected surface band gap, i.e., the Dirac gap, is observed near the TPT [21,24,25]. For $Bi_{2-x}In_xSe_3$, a broader TPT from TI to trivial insulator is reported, as suggested by transport and photoemission measurements on $Bi_{2-x}In_xSe_3$ thin films [26–28]. This linear gap-closure scenario motivates a study to characterize the evolution of the bulk bands of these two systems so as to fully understand the TPT [17,18]. While the SS has been characterized, observation of these bulk band features has not yet been reported. Therefore, to date, the underlying mechanism of non-magnetic-impurity-induced TPT still remains elusive. In order to obtain a much clearer insight into the mechanism, we performed systematic high-resolution angle-resolved photoemission spectroscopy (ARPES) measurements on $Bi_{2-x}In_xSe_3$ single crystals, focusing on the detailed evolution of both the bulk bands and the SS during the TPT.

In this paper, we report an observation of the phase transition from a TI to a trivial insulator in $Bi_{2-x}In_xSe_3$ single crystals with various nominal doping levels ($x = 0.05$, 0.10, 0.175, 0.225, and 0.30). We demonstrate that the bulk-gap size (∼0.50 eV) shows no significant change in the topologically nontrivial region (i.e., $x = 0.05$, 0.10, and 0.175), instead of a linear gap-closure behavior. The bulk gap appears to abruptly close at a specific doping level (∼0.175–0.225) accompanied by the complete suppression of the SS. After the TPT, the bulk-gap size increases for $x = 0.225$ and 0.30. Both the SOC and interactions upon band hybridization are suggested to cooperate in this local phase transition.

High-quality single crystals of $Bi_{2-x}In_xSe_3$ were grown by slowly cooling a stoichiometric mixture of high-purity elements of bismuth, indium, and selenium in an evacuated quartz tube [29]. ARPES measurements were performed at Renmin University of China and Institute of Physics, Chinese Academy of Sciences, with a He-discharge lamp, and at the

*Present address: Department of Physics, University of Science and Technology, Beijing, Beijing 100083, China.

†scw@ruc.edu.cn

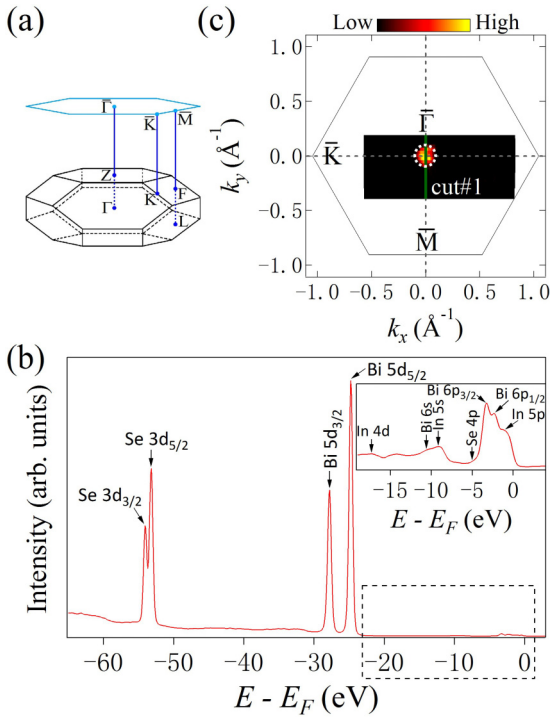

FIG. 1. (Color online) (a) Bulk BZ and its surface projection of $Bi_{2-x}In_xSe_3$. (b) Core-level photoemission spectrum ($h\nu = 100$ eV) of $x = 0.05$. The inset is a zoom-in of the VB from the dashed box. (c) ARPES intensity plot ($h\nu = 70$ eV) of $x = 0.05$ at E_F as a function of the 2D wave vector. The intensity is obtained by integrating the spectra within ±15 meV with respect to E_F. Cut 1 indicates the $\bar{\Gamma}\bar{M}$ direction, along which the data are presented in Fig. 2. The white dashed circle is a guide to the eyes, serving as the FS.

1-cubed ARPES end station at BESSY using synchrotron radiation. The overall angular and energy resolutions are better than 0.2 ° and 5 meV, respectively. Samples were cleaved *in situ* yielding flat (001) surfaces, and measured at $T \sim 10$ K, with a pressure better than 4×10^{-11} Torr.

The schematic bulk Brillouin zone (BZ) of $Bi_{2-x}In_xSe_3$ is presented in Fig. 1(a). As is shown in Fig. 1(b), well-defined peaks in the core-level photoemission spectrum of $x = 0.05$ demonstrate the high quality of the series of crystals used in this work. One can obtain insight into the binding energy within ~20 eV below E_F in the core-level spectrum, as shown in the inset of Fig. 1(b). Figure 1(c) shows the Fermi surface (FS) mapping data of $x = 0.05$ as a function of the in-plane wave vector.

Figure 2(a) shows the band dispersions of a series of doped samples along the $\bar{\Gamma}\bar{M}$ direction, indicated via cut 1 in Fig. 1(c). The corresponding second-derivative plots are shown in Fig. 2(b). The data were collected using an incident photon energy of 20 eV, ensuring the k_z positions close to the bulk Γ point [8,30]. Also, we verify the k_z dispersion of the band features by performing a photon-energy-dependent measurement (see Supplemental Material, Part 1) [31]. The plots in Fig. 2(a) clearly show the SS for $x \leqslant 0.175$, thus indicating a topologically nontrivial region, and the absence of the SS for $x \geqslant 0.225$, thus indicating a topologically trivial region. This could be further confirmed by the momentum-distribution curves (MDCs) of $x = 0.175$ and 0.225 shown in Figs. 2(c) and 2(d), respectively. The purely flat curves 1 and 2 in Fig. 2(d) are in great contrast to the well-dispersed spectra 1–4 in Fig. 2(c) from the linear dispersion of the SS. Due to the absence of the SS, the spectra 3 and 4 in $x = 0.225$ [Fig. 2(d)] could be reasonably assigned as the band dispersions of VB, with spectra 3 near the valance-band maximum (VBM) and spectra 4 deep in the VB. These band assignments are discussed in more detail in the Supplemental Material, Part 1 [31].

Furthermore, one can see the evolution of the bulk bands from Figs. 2(a) and 2(b). The bulk gap is defined as the difference between the conduction-band minimum (CBM) and the valley of VB at the $\bar{\Gamma}$ point for the topologically nontrivial region. The difference between the CBM and VBM is used for the topologically trivial region. In the topologically nontrivial region, the magnitude of bulk gaps reveal binding energies of 0.48, 0.50, and 0.49 eV for $x = 0.05$, 0.10, and 0.175, respectively, indicating no significant change upon doping. The valley structure in VB, caused by the band inversion, gradually weakens along with the increasing doping, demonstrating the decrease of SOC strength. This is quantitatively proven by the momentum of the bending band (δk) around the VBM, as marked by solid arrows in Figs. 2(a) and 2(b). The absolute values of the δk's are 0.091, 0.073, and 0.060 Å^{-1} for $x = 0.05$, 0.10, and 0.175, respectively. In the topologically trivial region, the band inversion disappears and the valley structure vanishes. The increase of the direct band gap indicates the further decrease of SOC strength [17,18]. Considering the evolution of both the SS and bulk band structures, we anticipate that a local phase transition characterized by a sudden gap closure happens close to $x \sim 0.175$–0.225. Another observation is that the Dirac point (DP) moves toward the CBM with the increasing doping. These can be expected to merge at the critical point, which also confirms the existence of a TPT [1,2].

The extracted evolution of the bulk gap is shown in Fig. 3(a). The gap size has a dramatic transformation between $x = 0.175$ and 0.225, as shown in the shadow region of Fig. 3(a), suggesting a critical transition. This behavior is in contrast to the mild change for $x = 0.05$, 0.10, and 0.175 (defined as negative values to distinguish from that in the topologically trivial phase). After crossing this apparent critical point, a strong increase from $x = 0.225$ to 0.30 is observed. This bulk-gap evolution deviates from that of the linear gap-closure scenario. The evident deviation shows that the underlying microscopic mechanism of TPT could not be simply elucidated by a SOC dominant effect. This systematic observation of the bulk band structure evolution suggests a different mechanism is present.

As proposed in Ref. [17], a band inversion is induced by SOC for a 3D TI. In the topologically nontrivial region, after turning on the SOC, there is a downward and upward shift of the CB and VB, respectively, causing the band inversion, and they hybridize with each other around the $\bar{\Gamma}$ point. Further, the bulk gap would be expected to reopen owing to the interactions within the overlap. Meanwhile, our observed bulk-gap behavior also indicates that the reopened bulk gap at the $\bar{\Gamma}$ point (i.e., the gap between the CBM and the valley) is no longer dominated by SOC alone. Therefore, the combined

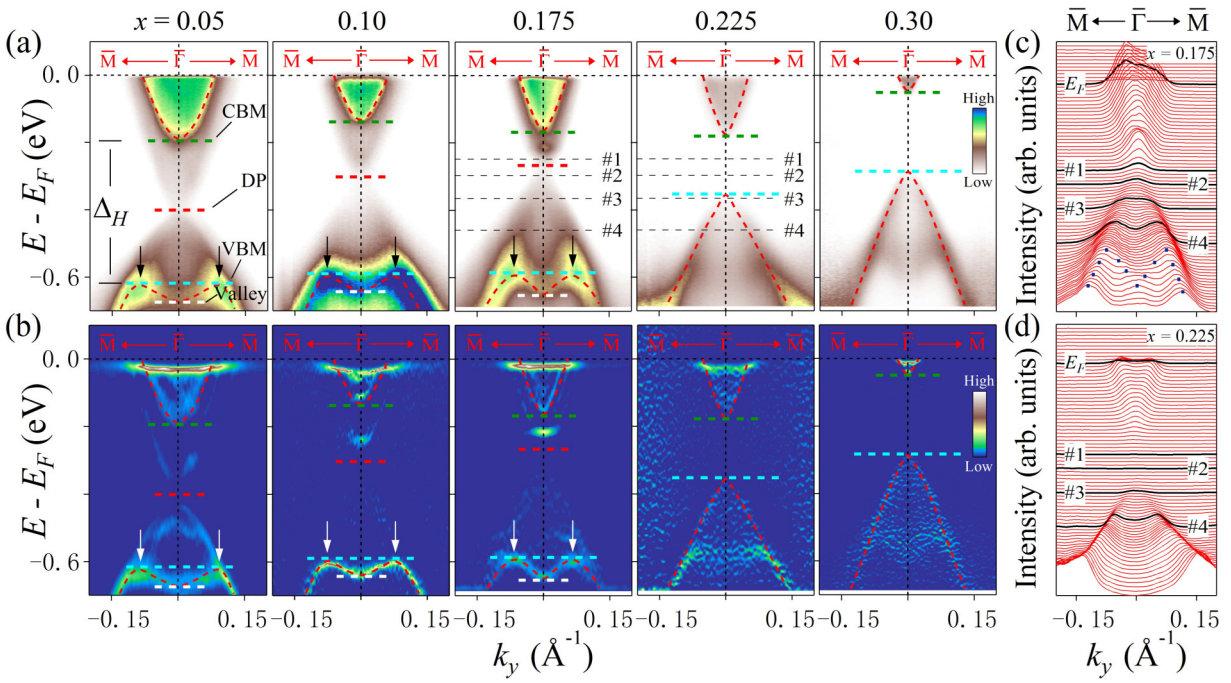

FIG. 2. (Color online) (a) ARPES intensity plots and (b) the corresponding second-derivative plots of $Bi_{2-x}In_xSe_3$ along the $\bar{\Gamma}\bar{M}$ direction ($h\nu = 20$ eV). The nominal composition value is noted above each representative plot. The CBM, VBM, DP, valley, and δk's are marked by green, blue, red, and white dashed lines, and solid arrows, respectively; the red dashed curves represent the bulk bands. Band dispersions are quantitatively determined by energy-distribution curve (EDC) and momentum-distribution curve (MDC) analysis and overlaid with the second-derivative plots. (c),(d) The corresponding MDC plots of $x = 0.175$ and 0.225 from (a), respectively. Spectra at the binding energies of -0.248, -0.297, -0.366, and -0.460 eV, as indicated by black dashes in (a), are highlighted by thick black curves. Blue dots in (c) are guides to the eyes for the valley structure.

effect of both SOC and interactions upon band hybridization should be taken as the determinant during the TPT.

It is possible to estimate the relative contribution from SOC and band hybridization. The overlap ratio (Δ_S) between the CB and VB after turning on the SOC is $\Delta_S = |E_g - E_{\mathrm{SOC}}|$, where E_g is the energy gap between the CBM and VBM before turning on the SOC and proportional to the covalent bonding strength within the quintuple layer [32], and E_{SOC} is the total-energy shift of the CB and VB caused by the SOC. The δk's of VB are exactly the momentum of the crossing points between the CB and VB when overlapping; thus, after the reopening, the indirect gap between the CBM and VBM [as shown in Fig. 2(a)] is defined as the hybridization gap (Δ_H). Therefore, we suggest that Δ_S, which corresponds to the relative strength of SOC, and Δ_H, which characterizes the interactions within the overlap, together modulate the evolution of the bulk gap in the topologically nontrivial region. In the topologically trivial region, the band inversion vanishes, along with the band hybridization ($\Delta_H \equiv 0$). As a consequence, the increase of the bulk-gap size is directly attributed to the decrease of SOC strength, i.e., Δ_S, upon In doping [17,18].

As is schematically illustrated in Fig. 3(b), we estimate Δ_S as follows: first, extracting the δk's of VB, shown as black vertical arrows; second, extrapolating the high-energy band dispersion to recover the unperturbed VB, and fitting the valley structure to get the unperturbed CB, shown as red dashed and purple solid curves, respectively; and last, by shifting the unperturbed CB upward and matching the crossing points, δk's, between the unperturbed CB and VB, we recover the overlap as the shadow area in the left panel. The energy difference between the extreme values of the red and green dashed curves is defined as Δ_S. (See more details in the Supplemental Material, Part 2 [31].)

In Fig. 3(c), the evolution of Δ_S and Δ_H is plotted as a function of In concentration. They have remarkably different tendencies in the topologically nontrivial phase, in which, upon In doping, Δ_S decreases monotonically, while Δ_H shows no noticeable change. We now discuss the possible combination of Δ_S and Δ_H in determining the bulk-gap size and thus try to understand the underlying mechanism of TPT. From a simple perspective, the bulk-gap value is the summation of Δ_H and the difference between the VBM and the valley. Therefore, a reasonable estimate of the bulk gap (Δ_E) using the experimental Δ_S and Δ_H values is $\Delta_E \approx \lambda \cdot \Delta_S + \Delta_H$, in which the factor λ characterizes the contribution from SOC. In the topologically nontrivial region, $\lambda = 0.4$, and in the topologically trivial region, $\lambda = 1.0$. By noticing that $\Delta_H \sim 0.4$ eV and $\Delta_S \sim 0.1$–0.2 eV in the topologically nontrivial phase, the gap size is seen to be dominated by Δ_H according to this formula. As a result, although Δ_S decreases faster along with increasing doping, the gap size changes slightly [as presented in the inset of Fig. 3(c)] at low In concentrations until the band inversion vanishes. Beyond the critical point, Δ_H vanishes, and thus the bulk gap is directly determined by the SOC strength, which decreases monotonically along with the increasing In concentration. This scenario reasonably addresses our observed bulk-gap

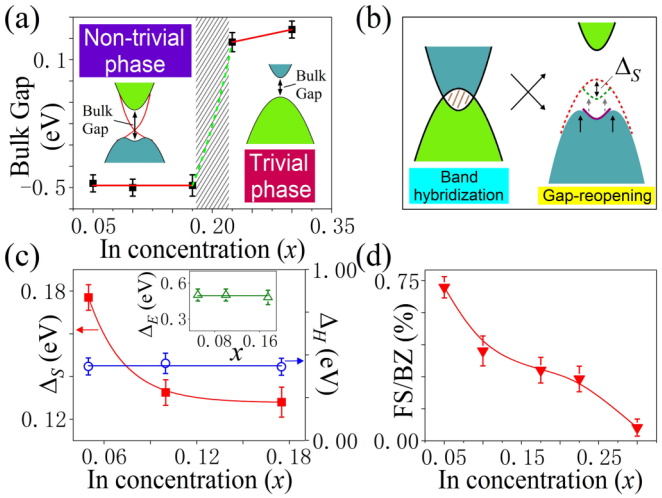

FIG. 3. (Color online) (a) The evolution of the bulk-gap size at the $\bar{\Gamma}$ point. The definition of the bulk gap in two phases is shown in the insets. The critical point is within the shadow region. (b) A schematic picture of bulk bands in band hybridization (left panel) and gap reopening (right panel) in the topologically nontrivial phase. The δk's (black vertical arrows), unperturbed VB (red dashed curve), unperturbed CB (purple solid curve), and shifted CB (green dashed curve) are indicated to enable an estimate of Δ_S. (c) Δ_S (red solid square) and Δ_H (blue open circle) as a function of x in the topologically nontrivial phase. The evolution of the estimated bulk gap, $\Delta_E \approx \lambda \cdot \Delta_S + \Delta_H$ ($\lambda = 0.4$) (green open triangle), upon doping is shown in the inset. (d) The doping dependence of the ratio of the enclosed FS area to the whole BZ.

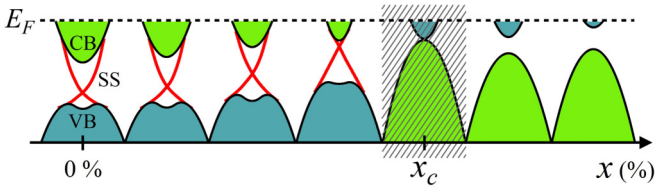

FIG. 4. (Color online) A schematic picture of the band structure evolution of $Bi_{2-x}In_xSe_3$ as a function of In concentration. The different colors of the bulk bands represent different orbital characters and parities.

evolution, and offers an important insight into the mechanism of TPT. Considering the behavior of Δ_H, we give a reasonable speculation here. According to the first-principles calculations of $Bi_{2-x}In_xSe_3$ proposed in Ref. [33], in the topologically trivial region, the CBM is composed of the Bi $6p$ and In $5s$ orbitals. Both of these orbitals are involved in the overlap between the CB and VB in the topologically nontrivial region. As the interactions upon band hybridization are proportional to the density of states (DOS) within the overlap, and considering the DOS is intimately connected with the overlap ratio, Δ_H may be expected to decrease along with the decreasing Δ_S. However, our observed nearly invariant Δ_H possibly indicates the non-negligible contribution of the increasing In $5s$ orbital in modulating the DOS within the overlap.

We estimate the carrier concentrations of our samples, by calculating the ratios of the enclosed FS area to the whole BZ, and present them in Fig. 3(d). This ratio decreases monotonically with increasing doping, agreeing well with the transport results proposed in Ref. [26].

A schematic picture of the band structure evolution during the TPT is conceptually sketched in Fig. 4. In the topologically nontrivial region ($x < x_c$), the band inversion exists, and thus the interactions upon band hybridization and SOC together modulate the bulk-gap size. As a result, the bulk gap shows no significant change. With the increase of In doping, the overlap ratio between the CB and VB decreases. At the critical point ($x = x_c$), the band inversion vanishes, as does the band hybridization, and the bulk gap collapses, accompanied by the vanishing of the SS. In the topologically trivial region ($x > x_c$), the further decreasing SOC strength separates the CB and VB, giving rise to the increase of bulk gap. The DP moves toward the CBM with the increasing doping, and the extrapolated merging point is at the vicinity of x_c. This behavior can be explained as a result of the reduction of the inverted band overlap ratio between the CB and VB.

To summarize, we have performed ARPES experiments on $Bi_{2-x}In_xSe_3$ single crystals to study the band structure evolution of the TPT induced by nonmagnetic impurities. We report the evolution of the bulk bands throughout the transition and propose a sudden gap-closure behavior across the phase transition, instead of the linear gap-closure scenario dominated by SOC alone. Our study suggests that the interactions upon band hybridization and SOC together determine the TPT, providing a different perspective on the underlying mechanism.

We thank Rong Yu and Xi Dai for helpful discussions, and Hechang Lei, Rui Cao, and Zongyao Zhang for their help with the x-ray diffraction measurements. This work was supported by grants from the National Science Foundation of China, National Basic Research Program of China (973 Program), Ministry of Education of China, China Academy of Science, and SSSTC. W.J. and R.M.O. were supported by the U.S. Department of Energy, Office of Basic Energy Sciences, Division of Materials Sciences and Engineering under Award Contract No. DE-FG 02-04-ER-46157. The work at Rutgers University was funded by the Gordon and Betty Moore Foundation's EPiQS Initiative through Grant No. GBMF4413 of the Rutgers Center for Emergent Materials.

R.L. and Z.L. contributed equally to this work.

[1] M. Z. Hasan and C. L. Kane, Rev. Mod. Phys. **82**, 3045 (2010).
[2] X.-L. Qi and S.-C. Zhang, Rev. Mod. Phys. **83**, 1057 (2011).
[3] L. Fu, C. L. Kane, and E. J. Mele, Phys. Rev. Lett. **98**, 106803 (2007).
[4] J. E. Moore and L. Balents, Phys. Rev. B **75**, 121306 (2007).
[5] D. Hsieh, Y. Xia, D. Qian, L. Wray, J. H. Dil, F. Meier, J. Osterwalder, L. Patthey, J. G. Checkelsky, N. P. Ong,

A. V. Fedorov, H. Lin, A. Bansil, D. Grauer, Y. S. Hor, R. J. Cava, and M. Z. Hasan, Nature (London) **460**, 1101 (2009).
[6] Y. L. Chen, J. G. Analytis, J.-H. Chu, Z. K. Liu, S.-K. Mo, X. L. Qi, H. J. Zhang, D. H. Lu, X. Dai, Z. Fang, S. C. Zhang, I. R. Fisher, Z. Hussain, and Z.-X. Shen, Science **325**, 178 (2009).
[7] D. Hsieh, Y. Xia, L. Wray, D. Qian, A. Pal, J. H. Dil, J. Osterwalder, F. Meier, G. Bihlmayer, C. L. Kane, Y. S. Hor, R. J. Cava, and M. Z. Hasan, Science **323**, 919 (2009).
[8] Y. Xia, D. Qian, D. Hsieh, L. Wray, A. Pal, H. Lin, A. Bansil, D. Grauer, Y. S. Hor, R. J. Cava, and M. Z. Hasan, Nat. Phys. **5**, 398 (2009).
[9] D. Hsieh, D. Qian, L. Wray, Y. Xia, Y. S. Hor, R. J. Cava, and M. Z. Hasan, Nature (London) **452**, 970 (2008).
[10] R. Roy, Phys. Rev. B **79**, 195322 (2009).
[11] P. Roushan, J. Seo, C. V. Parker, Y. S. Hor, D. Hsieh, D. Qian, A. Richardella, M. Z. Hasan, R. J. Cava, and A. Yazdani, Nature (London) **460**, 1106 (2009).
[12] P. Dziawa, B. J. Kowalski, K. Dybko, R. Buczko, A. Szczerbakow, M. Szot, E. Łusakowska, T. Balasubramanian, B. M. Wojek, M. H. Berntsen, O. Tjernberg, and T. Story, Nat. Mater. **11**, 1023 (2012).
[13] B. M. Wojek, P. Dziawa, B. J. Kowalski, A. Szczerbakow, A. M. Black-Schaffer, M. H. Berntsen, T. Balasubramanian, T. Story, and O. Tjernberg, Phys. Rev. B **90**, 161202(R) (2014).
[14] Z.-H. Pan, E. Vescovo, A. V. Fedorov, D. Gardner, Y. S. Lee, S. Chu, G. D. Gu, and T. Valla, Phys. Rev. Lett. **106**, 257004 (2011).
[15] I. A. Nechaev, R. C. Hatch, M. Bianchi, D. Guan, C. Friedrich, I. Aguilera, J. L. Mi, B. B. Iversen, S. Blügel, Ph. Hofmann, and E. V. Chulkov, Phys. Rev. B **87**, 121111(R) (2013).
[16] M. R. Scholz, J. Sánchez-Barriga, D. Marchenko, A. Varykhalov, A. Volykhov, L. V. Yashina, and O. Rader, Phys. Rev. Lett. **108**, 256810 (2012).
[17] H. Zhang, C.-X. Liu, X.-L. Qi, X. Dai, Z. Fang, and S.-C. Zhang, Nat. Phys. **5**, 438 (2009).
[18] B. A. Bernevig, T. L. Hughes, and S.-C. Zhang, Science **314**, 1757 (2006).
[19] L. Fu and C. L. Kane, Phys. Rev. B **76**, 045302 (2007).
[20] C.-X. Liu, X.-L. Qi, H. J. Zhang, X. Dai, Z. Fang, and S.-C. Zhang, Phys. Rev. B **82**, 045122 (2010).
[21] T. Sato, K. Segawa, K. Kosaka, S. Souma, K. Nakayama, K. Eto, T. Minami, Y. Ando, and T. Takahashi, Nat. Phys. **7**, 840 (2011).
[22] S. Xu, Y. Xia, L. Wray, S. Jia, F. Meier, J. H. Dil, J. Osterwalder, B. Slomski, A. Bansil, H. Lin, R. J. Cava, and M. Z. Hasan, Science **332**, 560 (2011).
[23] Y. L. Chen, Z. K. Liu, J. G. Analytis, J.-H. Chu, H. J. Zhang, B. H. Yan, S.-K. Mo, R. G. Moore, D. H. Lu, I. R. Fisher, S. C. Zhang, Z. Hussain, and Z.-X. Shen, Phys. Rev. Lett. **105**, 266401 (2010).
[24] S. Souma, M. Komatsu, M. Nomura, T. Sato, A. Takayama, T. Takahashi, K. Eto, K. Segawa, and Y. Ando, Phys. Rev. Lett. **109**, 186804 (2012).
[25] S. Xu, M. Neupane, I. Belopolski, C. Liu, N. Alidoust, G. Bian, S. Jia, G. Landolt, B. Slomski, J. H. Dil, P. P. Shibayev, S. Basak, T.-R. Chang, H.-T. Jeng, R. J. Cava, H. Lin, A. Bansil, and M. Z. Hasan, Nat. Commun. **6**, 6870 (2015).
[26] M. Brahlek, N. Bansal, N. Koirala, S.-Y. Xu, M. Neupane, C. Liu, M. Z. Hasan, and S. Oh, Phys. Rev. Lett. **109**, 186403 (2012).
[27] L. Wu, M. Brahlek, R. V. Aguilar, A. V. Stier, C. M. Morris, Y. Lubashevsky, L. S. Bilbro, N. Bansal, S. Oh, and N. P. Armitage, Nat. Phys. **9**, 410 (2013).
[28] Y. Watanabe, S. Kaneko, H. Kawazoe, and M. Yamane, Phys. Rev. B **40**, 3133 (1989).
[29] J. G. Analytis, J.-H. Chu, Y. L. Chen, F. Corredor, R. D. McDonald, Z. X. Shen, and I. R. Fisher, Phys. Rev. B **81**, 205407 (2010).
[30] M. Bianchi, D. Guan, S. Bao, J. L. Mi, B. B. Iversen, P. D. C. King, and P. Hofmann, Nat. Commun. **1**, 128 (2010).
[31] See Supplemental Material at http://link.aps.org/supplemental/10.1103/PhysRevB.92.115150 for photon-energy-dependent data, detailed discussions on the band assignments, and the estimate method of Δ_S.
[32] J. C. Slater and G. F. Koster, Phys. Rev. **94**, 1498 (1954).
[33] J. P. Liu and D. Vanderbilt, Phys. Rev. B **88**, 224202 (2013).